

Surface versus bulk Dirac state tuning in a three-dimensional topological Dirac semimetal

Madhab Neupane,^{1,2} Su-Yang Xu,¹ Nasser Alidoust,¹ Raman Sankar,³ Ilya Belopolski,¹ Daniel S. Sanchez,¹ Guang Bian,¹ Chang Liu,¹ Tay-Rong Chang,⁴ Horng-Tay Jeng,^{4,5} BaoKai Wang,^{6,7,8} Guoqing Chang,^{6,7} Hsin Lin,^{6,7} Arun Bansil,⁸ Fangcheng Chou,³ and M. Zahid Hasan^{1,9}

¹Joseph Henry Laboratory, Department of Physics, Princeton University, Princeton, New Jersey 08544, USA

²Condensed Matter and Magnet Science Group, Los Alamos National Laboratory, Los Alamos, New Mexico 87545, USA

³Center for Condensed Matter Sciences, National Taiwan University, Taipei 10617, Taiwan

⁴Department of Physics, National Tsing Hua University, Hsinchu 30013, Taiwan

⁵Institute of Physics, Academia Sinica, Taipei 11529, Taiwan

⁶Centre for Advanced 2D Materials and Graphene Research Centre, National University of Singapore, 6 Science Drive 2, Singapore 117546

⁷Department of Physics, National University of Singapore, 2 Science Drive 3, Singapore 117542

⁸Department of Physics, Northeastern University, Boston, Massachusetts 02115, USA

⁹Princeton Center for Complex Materials, Princeton University, Princeton, New Jersey 08544, USA

(Received 4 January 2015; revised manuscript received 6 June 2015; published 24 June 2015)

Recently, a crystalline-symmetry-protected three-dimensional (3D) bulk Dirac semimetal phase has been experimentally identified in a stoichiometric high-mobility compound, Cd_3As_2 . The Dirac state observed in Cd_3As_2 has been attributed to originate mostly from the bulk state while calculations show that the bulk and surface states overlap over the entire Dirac dispersion energy range. In this study we unambiguously reveal doping induced evolution of the ground state of surface and bulk electron dynamics in a 3D Dirac semimetal. The technique demonstrated in this study by simultaneously using angle-resolved photoemission spectroscopy (ARPES) and *in situ* surface deposition isolates the surface and bulk states in Cd_3As_2 . Our experimental results provide a method for tuning the chemical potential as well as to observe surface states degenerate with bulk states, which will be useful for future applications of a 3D Dirac semimetal.

DOI: [10.1103/PhysRevB.91.241114](https://doi.org/10.1103/PhysRevB.91.241114)

PACS number(s): 73.20.At

Two-dimension (2D) Dirac electron systems often exhibit exotic quantum phenomena and, therefore, have been considered as one of the central topics in modern condensed matter physics. The most promising examples are the extensive studies on graphene and the surface states of topological insulators (TIs) [1–11]. Dirac semimetals have gapless linear dispersions in three spatial dimensions, which can be regarded as a 3D analog of graphene. Recently, 3D Dirac semimetals have been theoretically predicted [12,13] and experimentally realized in Cd_3As_2 [14–17] and Na_3Bi [18–20]. These Dirac semimetals possess two Dirac nodes which are protected by the crystalline symmetry and are believed to hold the key for realizing exotic Weyl physics [12–27]. It has been theoretically understood that a 3D Dirac node can be viewed as a composite of two sets of distinct Weyl fermions [13,21]. Moreover, if time-reversal or space inversion symmetry is broken, then the theory predicts that the 3D Dirac point (DP) can split into two Weyl nodes that are separated in momentum space. Thus, a Weyl semimetal phase can be realized, which can be described by Weyl nodes at the Fermi level for the bulk and the presence of the exotic spin-polarized Fermi arcs on the surfaces connecting the bulk nodes [13].

The Dirac state observed in the Cd_3As_2 system has been attributed to originate, mostly, from the bulk states [13–15] where the Dirac dispersion varies with photon energy [14,15]. Also, spin-resolved angle-resolved photoemission spectroscopy (SR-ARPES) measurements show negligible spin polarization [14] suggesting its bulk origin. However, calculations show that the bulk and surface states overlap on the entire Dirac dispersion energy range [13,14]. Therefore, it is natural to ask a question: How can the surface state be resolved in the Cd_3As_2 system? Furthermore, the overlapping of the

surface and bulk bands may cause the hybridization between them, which makes it difficult to separate the contributions of the surface and bulk states. Hence, it is important to develop a technique to enhance the spectral weight of the surface states in Cd_3As_2 .

In this study we report the realization of the doping induced evolution of the ground state of surface and bulk electron dynamics in a 3D Dirac semimetal. A methodology demonstrated here isolates the surface and bulk states in a high-mobility stoichiometric 3D Dirac semimetal Cd_3As_2 . Using high-resolution angle-resolved photoemission spectroscopy (ARPES) and *in situ* alkali metal surface deposition, we show that Cd_3As_2 features a bulk Dirac cone located at the center of the (001) surface Brillouin zone (BZ). This surface doping induced tunability of the surface chemical potential reveals between the variation of surface versus bulk Dirac dispersion. The novel and somewhat unexpected effect of surface deposition provides an entirely novel approach to selectively probe bulk and surface states in systems where these are degenerate. Our measurement provides a beautiful application of this procedure to the study of the (001) surface state of Cd_3As_2 .

Single crystalline samples of Cd_3As_2 used in this study were grown using the standard method, which is described elsewhere [28]. ARPES measurements for the low energy electronic structure were performed at the beamlines 4.0.3 and 12.0.1 at the Advanced Light Source (ALS) in Berkeley California, equipped with high efficiency VG-Scienta R8000 and R200 electron analyzers. Samples were cleaved *in situ* and measured at 10 K in a vacuum better than 1×10^{-10} torr. The energy resolution was 10–30 meV and the angular resolution was better than 0.2° for all synchrotron-based ARPES

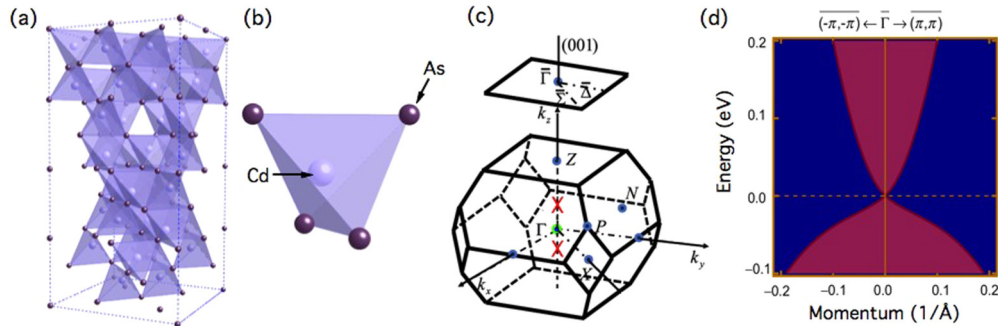


FIG. 1. (Color online) Crystal structure. (a) Cd_3As_2 crystallizes in a tetragonal body center structure with a space group of $I4_1cd$, which has 32 formula units in the unit cell. (b) The basic structure unit is a four corner-sharing CdAs_3 -trigonal pyramid. (c) The bulk Brillouin zone (BZ) and the projected surface BZ along the (001) direction. The red crossings locate at $(k_x, k_y, k_z) = (0, 0, 0.15 \frac{2\pi}{c^*})$ ($c^* = c/a$). (d) First-principles calculation of the bulk electronic structure. Projected bulk band structure on to the (001) surface, where the shaded area shows the projection of the bulk bands.

measurements. Samples were observed to be stable and, for a typical 20 h measurement period, unsusceptible to degradation. Sodium deposition was performed at the beamline 4.0.1 of the ALS from SAES getter source (SAES Getters USA, Inc.), which was thoroughly degassed before starting the experiment. During deposition, pressure in the experimental chamber was $< 1 \times 10^{-10}$ torr. First-principles calculations were based on the generalized gradient approximation (GGA) [29] using the projector augmented wave method [30] as implemented in the VASP package [31]. The experimental crystal structure was used [28]. The electronic structure calculations were performed over $4 \times 4 \times 2$ Monkhorst-Pack k mesh with the spin-orbit coupling included self-consistently.

We start our discussion by reviewing the crystal structure and the Brillouin zone (BZ) of Cd_3As_2 . The crystal structure of Cd_3As_2 has a tetragonal unit cell with $a = 12.67 \text{ \AA}$, $c = 25.48 \text{ \AA}$, $Z = 32$, and the space group of $I4_1cd$ [see Figs. 1(a) and 1(b)]. In this structure, arsenic ions are approximately cubic close packed and Cd ions are tetrahedrally coordinated. Each As ion is surrounded by Cd ions at six of the eight corners of a distorted cube [see Fig. 1(b)], with the two vacant sites located at the diagonally opposite corners of a cube face [28]. The corresponding BZ is shown in Fig. 1(c), where the center of the BZ is the Γ point, the centers of the top and bottom square surfaces are the Z points, and other high symmetry points are also noted. In electrical transport measurements, Cd_3As_2 has long attracted much attention because of its very high electron mobility up to $\simeq 10^5 \text{ cm}^2 \text{ V}^{-1} \text{ s}^{-1}$ [32] and interesting magnetotransport properties including a very small effective mass [33]. In theoretical calculations, Cd_3As_2 is of further interest because it is believed to have an inverted band structure [34]. More interestingly, a very recent theoretical study [13] has shown that spin-orbit interaction in Cd_3As_2 cannot open up a full energy gap between the inverted bulk conduction and valence bands due to the protection of an additional crystallographic symmetry [22] (in the case of Cd_3As_2 it is the C_4 rotational symmetry along the k_z direction [13]), which is in contrast to other band-inverted systems such as Bi_2Se_3 class [3]. Theory predicts [13] that the C_4 rotational symmetry protects two bulk (3D) Dirac band touchings at two special \mathbf{k} points along the Γ -Z momentum space cut direction, as shown by the red crossings in Fig. 1(c).

At the (001) surface, theoretical calculations show the presence of one 3D Dirac cone at the BZ center point ($\bar{\Gamma}$) as shown in Fig. 1(d). Therefore, Cd_3As_2 offers a platform for an exotic space group symmetry-protected bulk Dirac semimetal (BDS) phase, which additionally features a very high carrier mobility and an inverted band structure.

We systematically study the electronic structure of Cd_3As_2 at the cleaved (001) surface by successive Na deposition. High-resolution ARPES dispersion measurements are performed in the close vicinity of the Fermi level as shown in Fig. 2. The used photon energy of 102 eV corresponds to the photon energy at which bulk Dirac dispersion is observed. At this “magic” photon energy, a linearly dispersive Dirac cone is observed at the surface BZ center $\bar{\Gamma}$ point, whose Dirac node is found to be located at binding energy of $E_B \simeq 0.2 \text{ eV}$. At the Fermi level, only the upper Dirac band but no other electronic states are observed. On the other hand, the lower Dirac cone is found to coexist with a parabolic bulk valence band, which can be seen from Fig. 2(a). Thus the data are consistent with recent results [14,15] and theoretical calculations [13]. In theory, there are two 3D Dirac nodes that are expected at two special \mathbf{k} points along the Γ -Z momentum space cut direction, as shown by the red crossings in Fig. 1(d). At the (001) surface, these two \mathbf{k} points along the Γ -Z axis project on to the $\bar{\Gamma}$ point of the (001) surface BZ [Fig. 1(d)]. Therefore, at the (001) surface, theory predicts the existence of one 3D Dirac cone at the BZ center $\bar{\Gamma}$ point, as shown in Fig. 2(a).

More substantial changes are observed by the *in situ* surface deposition of alkali metal (sodium, Na) on the cleaved surfaces of Cd_3As_2 . As a function of Na-deposition time, three stages can be identified. At first for moderate Na deposition (~ 90 s) the Dirac point (DP) moves to higher binding energy by electron doping and a sharper state is observed to emerge at the edge of the bulk continuum. We can identify this stage at which surface states start to develop. For intermediate Na deposition (~ 90 to 120 s, Fig. 2 middle panel), the electron doping further increases and sharper boundary states appear. This stage corresponds with fully developed surface states. We estimated about 1 ML coverage of Na on the surface of Cd_3As_2 after 120 s of surface deposition. Finally, heavy Na deposition (beyond 180 s) leaves the surface states and DP unchanged, which indicates that the sample cannot be

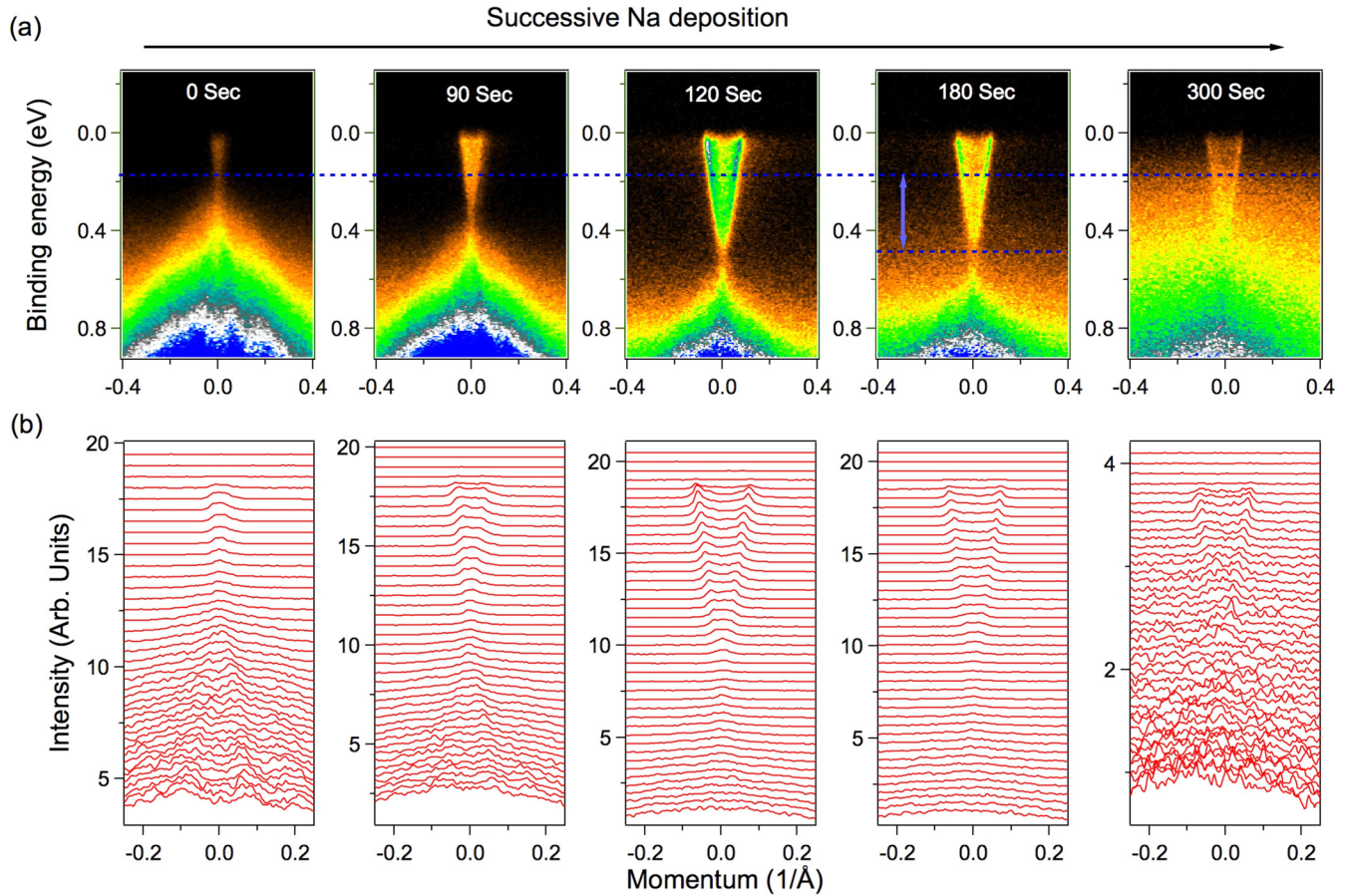


FIG. 2. (Color online) Fermi level tuning by surface Na deposition. (a) ARPES dispersion map with successive Na deposition. The time for Na deposition is noted on spectra. Dirac-cone-like intensity continuum is observed for no surface deposition spectrum. Long (short) blue dashed line shows the binding energy position of the Dirac point without (with) surface deposition. And vertical arrow indicates the energy shift of the binding energy (~ 300 meV). These data were measured with photon energy of 102 eV and temperature of 10 K at ALS BL4. (b) Corresponding momentum distribution curves (MDCs).

further doped. These observations are further illustrated by the momentum distribution curves (MDCs) plotted in Fig. 2(b).

In order to directly visualize the isolation of the surface and bulk states in Cd_3As_2 , we compare MDCs extracted from 50 meV binding energy at different deposition times (see Fig. 3). It is worth noting that the topological Dirac SM carries a nontrivial 2D Z_2 invariant on either the $k_z = 0$ or the $k_z = \pi$ plane. Therefore, the Dirac semimetal turns into a strong Z_2 topological insulator if an external perturbation breaks the C_4 symmetry but does not break time-reversal symmetry [35]. Thus the projected state on the (001) surface gives both bulk and surface states, as shown schematically in Fig. 3(a). The MDCs at different deposition times are shown in Fig. 3(c), whereas the white dashed line on the ARPES spectra in Fig. 3(b) depicts the approximate energy position of the extracted MDCs. From Fig. 3(c) it is evident that after deposition the double peaks emerge from a single peak of MDC before deposition. These two peaks correspond to the surface state of linear dispersion.

In order to illustrate the surface state nature of the dispersion after deposition, we perform photon energy dependent ARPES measurement as shown in Fig. 4. For this purpose, we use a relatively p -type sample where the chemical potential is located in the vicinity of the DP (see Fig. 4). A 3D Dirac

semimetal is shown to feature nearly linear dispersions along all three-momentum space directions close to the crossing point, even though Fermi velocity can vary significantly along different directions [14]. With the introduction of *in situ* Na deposition of ~ 120 s, the chemical potential is shifted up by 300 meV, leaving the upper cone now visible. Furthermore, the boundaries of the upper dispersion maps seem to be sharper. To identify their origin, we perform photon energy dependent measurements from 96 to 110 eV with a 2 eV energy increment (see Fig. 4). Upon varying the photon energy, the resulting dispersion maps are found to be unchanged, which is evidence supporting their 2D nature (see Fig. 4). These measurements further support our claim, which is that the precise control of the carrier density, and, therefore, the desired Fermi level, can be achieved in the Cd_3As_2 system.

Now we discuss some interesting consequences of our experiment. First, the surface alkali metal deposition on Cd_3As_2 has revealed that the chemical potential can be tuned, at least near the surface since ARPES is relatively surface sensitive. Second, before the surface deposition, the bulk Dirac cone shows intensity filled inside the cone. The outer boundary of the bulk Dirac cone dispersion, which mostly represents the surface states, is observed to become brighter and sharper after Na deposition (see Figs. 2 and 4). Thus, the deposition of the

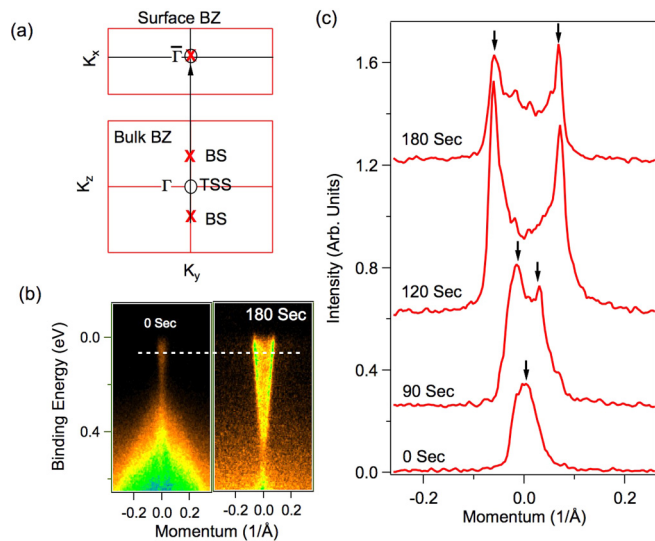


FIG. 3. (Color online) Surface vs bulk state tuning. (a) Schematic view of the surface and bulk BZ along (001) plane. The red x sign shows the bulk Dirac cone and circle sign denote the topological surface state. BS and TSS represent bulk Dirac state and topological surface states. (b) ARPES measured surface dispersion maps of Cd_3As_2 . The deposition time is noted on the spectra. The white dashed line represents the approximate binding energy position for the extracted momentum distribution curves (MDCs). (c) MDCs extracted from the spectra measured with different deposition times. The arrow lines represent the peak position. The evolution of the double peaks from a single peak shows how the spectral weight mostly dominated by surface states arise from the bulk state.

alkali metal on the cleaved surface of Cd_3As_2 can serve as a methodology to isolate the surface and bulk bands in this system. Third, our photon energy dependent measurements reveal that the surface deposition provides a technique for tuning the bulk versus surface state. By the addition of Na on the surface of Cd_3As_2 , the ARPES signal becomes more surfacelike, which may probably be due to decreasing the penetration depth of the photon flux. We note that quantum wells states should appear after the Na deposition on the surface of the Cd_3As_2 due to the bulk band bending. But, the quantum well state should not remain gapless, but should gap out. This is a fundamental point and cannot be explained by a quantum well state. Furthermore, the surface state shows no evolution as a function of Na deposition, which is not typical for quantum well states but is entirely consistent with the topological surface state. Lastly, our observation of this state is entirely consistent with first-principles calculations [Fig. 1(d)] and our photon energy dependence ARPES measurements (Fig. 4). Moreover, our data are highly dominated by the sharper boundary states over the entire binding energy range from Dirac point to the Fermi level.

In conclusion, we observe a novel and somewhat unexpected effect of surface deposition on Cd_3As_2 , providing an entirely new method to selectively probe bulk and surface states in systems where these are degenerate. We apply this technique to observe the first topological surface state in Cd_3As_2 and the first surface state in any compound which is degenerate with the bulk bands. This work can be applied to the study of other surface states, trivial or topological, degenerate with bulk bands, to better understand surface electronic structures in condensed matter systems.

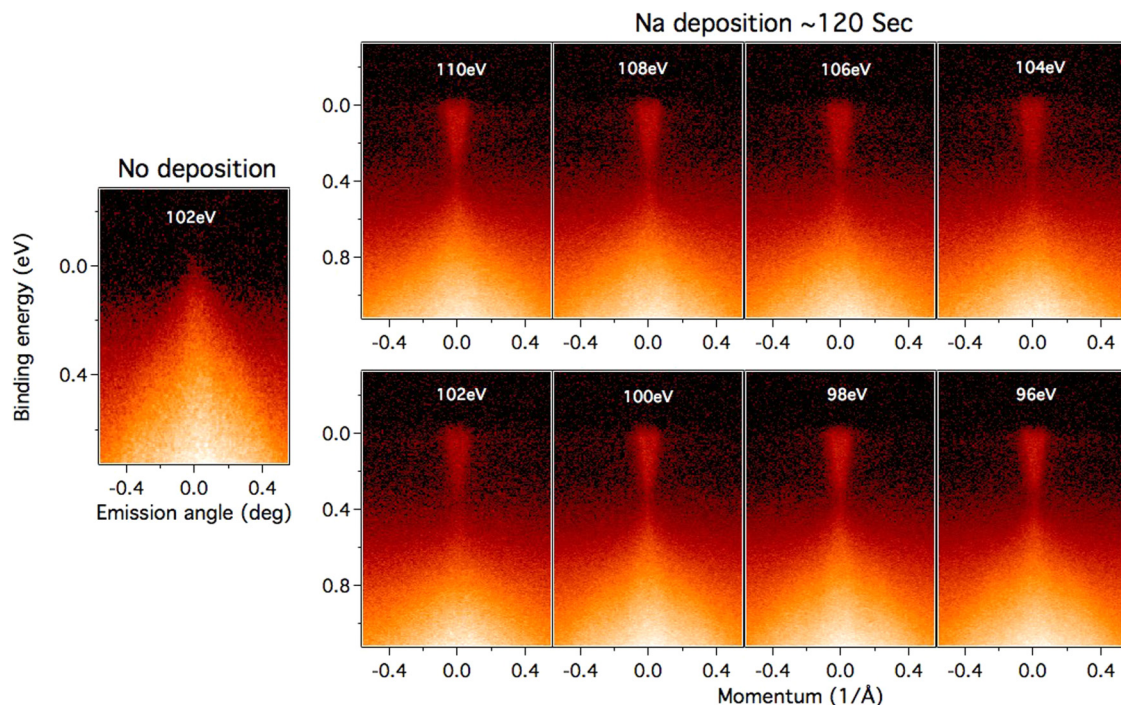


FIG. 4. (Color online) Observation of surface state. ARPES dispersion maps measured before and after Na deposition. The sample measured here is relatively *p* type, which is prepared under slightly different growth conditions (temperature and growth time). Photon energy dependent ARPES dispersion maps after 120 s of Na deposition. The measured photon energies are noted on the spectra. These data were collected at a temperature of 10 K.

Work at Princeton University is supported by the US National Science Foundation Grant, NSF-DMR-1006492. M.Z.H. acknowledges visiting-scientist support from Lawrence Berkeley National Laboratory and additional partial support from the A. P. Sloan Foundation and NSF-DMR-0819860. The work at Northeastern University was supported by the US Department of Energy (DOE), Office of Science, Basic Energy Sciences Grant No. DE-FG02-07ER46352, and benefited from Northeastern University's Advanced Scientific Computation Center (ASCC) and the NERSC supercomputing center through DOE Grant No. DE-AC02-05CH11231. M.N. at LANL

acknowledges support from LANL LDRD program. H.L. acknowledges the Singapore National Research Foundation for support under NRF Grant No. NRF-NRFF2013-03. T.-R.C. and H.-T.J. are supported by the National Science Council, Taiwan. H.-T.J. also thanks NCHC, CINC-NTU, and NCTS, Taiwan, for technical support. We thank J. D. Denlinger and A. V. Fedorov for beamline assistance at the Advanced Light Source (ALS-LBNL) in Berkeley. M.N. acknowledges discussion with Tomasz Durakiewicz from LANL, and A. Alexandradinata and Z. Wang from Princeton Physics.

-
- [1] P. A. M. Dirac, *Proc. R. Soc. London Ser. A* **117**, 610 (1928).
- [2] A. K. Geim and K. S. Novoselov, *Nat. Mater.* **6**, 183 (2007).
- [3] M. Z. Hasan and C. L. Kane, *Rev. Mod. Phys.* **82**, 3045 (2010).
- [4] X.-L. Qi and S.-C. Zhang, *Rev. Mod. Phys.* **83**, 1057 (2011).
- [5] M. Z. Hasan, S.-Y. Xu, and M. Neupane, *Topological Insulators: Fundamentals and Perspectives* (John Wiley and Sons, New York, 2015).
- [6] D. Hsieh, D. Qian, L. Wray, Y. Xia, Y. S. Hor, R. J. Cava, and M. Z. Hasan, *Nature (London)* **452**, 970 (2008).
- [7] Y. Xia, D. Qian, D. Hsieh, L. Wray, A. Pal, H. Lin, A. Bansil, D. Grauer, Y. S. Hor, R. J. Cava, and M. Z. Hasan, *Nat. Phys.* **5**, 398 (2009).
- [8] Y. L. Chen, J. G. Analytis, J.-H. Chu, Z. K. Liu, S.-K. Mo, X. L. Qi, H. J. Zhang, D. H. Lu, X. Dai, Z. Fang, S. C. Zhang, I. R. Fisher, Z. Hussain, and Z.-X. Shen, *Science* **325**, 178 (2009).
- [9] M. Neupane, S.-Y. Xu, L. A. Wray, A. Petersen, R. Shankar, N. Alidoust, Chang Liu, A. Fedorov, H. Ji, J. M. Allred, Y. S. Hor, T.-R. Chang, H.-T. Jeng, H. Lin, A. Bansil, R. J. Cava, and M. Z. Hasan, *Phys. Rev. B* **85**, 235406 (2012).
- [10] Su-Yang Xu, Y. Xia, L. A. Wray, S. Jia, F. Meier, J. H. Dil, J. Osterwalder, B. Slomski, A. Bansil, H. Lin, R. J. Cava, and M. Z. Hasan, *Science* **332**, 560 (2011).
- [11] M. Neupane, N. Alidoust, S.-Y. Xu, T. Kondo, Y. Ishida, D. J. Kim, Chang Liu, I. Belopolski, Y. J. Jo, T.-R. Chang, H.-T. Jeng, T. Durakiewicz, L. Balicas, H. Lin, A. Bansil, S. Shin, Z. Fisk, and M. Z. Hasan, *Nat. Commun.* **4**, 2991 (2013).
- [12] Z. Wang, Y. Sun, X. Q. Chen, C. Franchini, G. Xu, H. Weng, X. Dai, and Z. Fang, *Phys. Rev. B* **85**, 195320 (2012).
- [13] Z. Wang, H. Weng, Q. Wu, X. Dai, and Z. Fang, *Phys. Rev. B* **88**, 125427 (2013).
- [14] M. Neupane, S.-Y. Xu, R. Sankar, N. Alidoust, G. Bian, C. Liu, I. Belopolski, T.-R. Chang, H.-T. Jeng, H. Lin, A. Bansil, F. Chou, and M. Z. Hasan, *Nat. Commun.* **5**, 3786 (2014).
- [15] S. Borisenko, Q. Gibson, D. Evtushinsky, V. Zabolotnyy, B. Buchner, and R. J. Cava, *Phys. Rev. Lett.* **113**, 027603 (2014).
- [16] Z. K. Liu, J. Jiang, B. Zhou, Z. J. Wang, Y. Zhang, H. M. Weng, D. Prabhakaran, S.-K. Mo, H. Peng, P. Dudin, T. Kim, M. Hoesch, Z. Fang, X. Dai, Z. X. Shen, D. L. Feng, Z. Hussain, and Y. L. Chen, *Nat. Mater.* **13**, 677 (2014).
- [17] H. Yi, Z. Wang, C. Chen, Y. Shi, Y. Feng, A. Liang, Z. Xie, S. He, J. He, Y. Peng, X. Liu, Y. Liu, L. Zhao, G. Liu, X. Dong, Jun Zhang, M. Nakatake, M. Arita, K. Shimada, H. Namatame, M. Taniguchi, Z. Xu, C. Chen, X. Dai, Z. Fang, and X. J. Zhou, *Sci. Rep.* **4**, 6106 (2014).
- [18] Z. K. Liu, B. Zhou, Y. Zhang, Z. J. Wang, H. M. Weng, D. Prabhakaran, S.-K. Mo, Z. X. Shen, Z. Fang, X. Dai, Z. Hussain, and Y. L. Chen, *Science* **343**, 864 (2014).
- [19] S.-Y. Xu, C. Liu, S. K. Kushwaha, T.-R. Chang, J. W. Krizan, R. Sankar, C. M. Polley, J. Adell, T. Balasubramanian, K. Miyamoto, N. Alidoust, Guang Bian, M. Neupane, I. Belopolski, H.-T. Jeng, C.-Y. Huang, W.-F. Tsai, H. Lin, F. C. Chou, T. Okuda, A. Bansil, R. J. Cava, and M. Z. Hasan, [arXiv:1312.7624](https://arxiv.org/abs/1312.7624).
- [20] S.-Y. Xu, C. Liu, S. K. Kushwaha, R. Sankar, J. W. Krizan, I. Belopolski, M. Neupane, G. Bian, N. Alidoust, T.-R. Chang, H.-T. Jeng, C.-Y. Huang, W.-F. Tsai, H. Lin, P. P. Shibayev, F.-C. Chou, R. J. Cava, and M. Z. Hasan, *Science* **347**, 294 (2015).
- [21] S. Murakami, *New J. Phys.* **9**, 356 (2007).
- [22] S. M. Young, S. Zaheer, J. C. Y. Teo, C. L. Kane, E. J. Mele, and A. M. Rappe, *Phys. Rev. Lett.* **108**, 140405 (2012).
- [23] H. Weyl, *Phys.* **56**, 330 (1929).
- [24] G. T. Volovik, *JETP Lett.* **75**, 55 (2002).
- [25] Z. Fang, N. Nagaosa, K. S. Takahashi, A. Asamitsu, R. Mathieu, T. Ogasawara, H. Yamada, M. Kawasaki, Y. Tokura, and K. Terakura, *Science* **302**, 92 (2003).
- [26] X. Wan, A. M. Turner, A. Vishwanath, and S. Y. Savrasov, *Phys. Rev. B* **83**, 205101 (2011).
- [27] G. B. Halasz and L. Balents, *Phys. Rev. B* **85**, 035103 (2012).
- [28] G. A. Steigmann and J. Goodyear, *Acta Crystallogr. Sect. B* **24**, 1062 (1968).
- [29] J. P. Perdew, K. Burke, and M. Ernzerhof, *Phys. Rev. Lett.* **77**, 3865 (1996).
- [30] P. E. Blochl, *Phys. Rev. B* **50**, 17953 (1994); G. Kresse and D. Joubert, *ibid.* **59**, 1758 (1999).
- [31] G. Kresse and J. Hafner, *Phys. Rev. B* **48**, 13115 (1993); G. Kresse and J. Furthmüller, *Comput. Mater. Sci.* **6**, 15 (1996); *Phys. Rev. B* **54**, 11169 (1996).
- [32] J.-P. Jay-Gerin, M. J. Aubin, and L. G. Caron, *Solid State Commun.* **21**, 771 (1977).
- [33] W. Zdanowicz, *Thin Solid Films* **61**, 41 (1979).
- [34] B. D. Plenkiewicz and P. Plenkiewicz, *Phys. Status Solidi B* **94**, K57 (2006).
- [35] B.-J. Yang and N. Nagaosa, *Nat. Commun.* **5**, 4898 (2014).